Eur. Phys. J. C (2019) 79:467
https://doi.org/10.1140/epjc/s10052-019-6955-5

THE EUROPEAN PHYSICAL JOURNAL C

Regular Article - Theoretical Physics

Signs of heavy Higgs bosons at CLIC: an e^+e^- road to the electroweak phase transition

J. M. No[1,2,a], **M. Spannowsky**[3,b]

[1] Department of Physics, King's College London, Strand, London WC2R 2LS, UK
[2] Departamento de Fisica Teorica and Instituto de Fisica Teorica, IFT-UAM/CSIC, Cantoblanco, 28049 Madrid, Spain
[3] Physics Department, Institute of Particle Physics Phenomenology, Durham University, Durham DH1 3LE, UK

Received: 25 October 2018 / Accepted: 17 May 2019 / Published online: 4 June 2019

Abstract We analyse the sensitivity of the proposed compact linear collider (CLIC) to the existence of beyond the standard model (SM) Higgs bosons through their decays into pairs of massive gauge bosons $H \to VV$ and SM-like Higgses $H \to hh$, considering CLIC centre of mass energies $\sqrt{s} = 1.4$ TeV and 3 TeV. We find that resonant di-Higgs searches at CLIC would allow for up to two orders of magnitude improvement w.r.t. the sensitivity achievable by HL-LHC in the mass range $m_H \in [250\,\text{GeV}, 1\,\text{TeV}]$. Focusing then on a real singlet extension of the SM, we explore the prospects of heavy Higgs searches at CLIC for probing the regions of parameter space yielding a strongly first order electroweak phase transition that could generate the observed matter-antimatter asymmetry of the Universe. Our study illustrates the complementarity between CLIC and other possible future colliders like FCC-*ee* in probing singlet extensions of the SM, and shows that high-energy e^+e^- colliders provide a powerful means to unravel the nature of electroweak symmetry breaking in the early Universe.

Contents

[a] e-mail: Josemiguel.no@uam.es
[b] e-mail: Michael.Spannowsky@durham.ac.uk

1 Introduction

A key goal of the present and future collider physics programme is to reveal the structure of the (scalar) sector responsible for electroweak symmetry breaking (EWSB) in Nature. While ongoing ATLAS and CMS analyses at the Large Hadron Collider (LHC) show that the properties of the discovered Higgs particle are close to those expected for the standard model (SM) Higgs boson h [1–3], it still needs to be determined whether the scalar sector is realised in its most minimal form, i.e. consisting of one $SU(2)_L$ doublet, or has a richer structure, containing additional states. Non-minimal scalar sectors are very well-motivated, arising naturally in the context of weakly coupled completions of the SM that address the hierarchy problem. At the same time, extensions of the SM scalar sector could provide the means to address a key open question at the interface of particle physics and cosmology, namely the generation of the cosmic matter-antimatter asymmetry, via electroweak (EW) baryogenesis [4].

Among the proposed future collider experiments, the compact linear collider (CLIC) would be a multi-TeV e^+e^- collider [5,6], combining the high-energy reach with the clean collision environment of an electron-positron machine. CLIC would operate in three energy stages, corresponding to centre of mass (c.o.m.) energies $\sqrt{s} = 380$ GeV, 1.4 TeV, 3 TeV, providing an ideal setup to study the properties of the Higgs

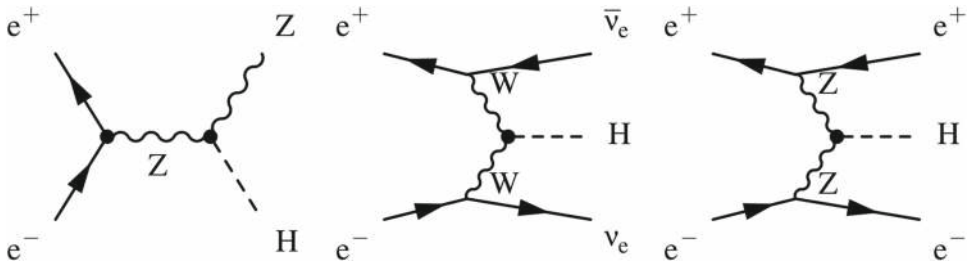

Fig. 1 Feynman diagrams for the three dominant Higgs boson production modes: $e^+e^- \to HZ$ (left), $e^+e^- \to H\nu\nu$ (middle) and $e^+e^- \to He^+e^-$ (right)

sector. In this respect, very sensitive direct probes of the existence of new, heavier Higgs bosons, possible with $\sqrt{s} = 1.4$ TeV and 3 TeV c.o.m. energy configurations, are highly complementary to precise measurements of the properties of the 125 GeV Higgs boson, and may yield the dominant probe of a non-standard Higgs sector.

In this work we analyse the reach of CLIC in searching for heavy Higgs bosons which decay to a pair of massive gauge bosons $VV = W^+W^-, ZZ$ or a pair of 125 GeV Higgs bosons. This allows to assess the direct sensitivity of CLIC to non-minimal Higgs sectors, and to compare it with that of the HL-LHC, providing at the same time a benchmark for sensitivity comparison with other possible future high-energy collider facilities like FCC(-*ee* and -*hh*). In addition, we assess the capability of CLIC heavy Higgs searches in probing the nature of the EW phase transition in the context of a general real singlet scalar extension of the SM [7–9]. This scenario can capture the phenomenology of the Higgs sector in more complete theories beyond the SM such as the NMSSM (see [10] and references therein) or Twin Higgs theories [11]. At the same time, the singlet scalar extension of the SM constitutes a paradigm for achieving a strongly first order EW phase transition that could generate the observed matter-antimatter asymmetry of the Universe.

The paper is organised as follows: in Sect. 2 we discuss the main aspects of Higgs production at CLIC, as well as the various computational tools we use for our analysis. In Sect. 3 we assess the CLIC sensitivity in direct searches of heavy scalars decaying into EW gauge boson pairs. In Sect. 4 we focus instead on heavy scalar decays into a pair of 125 GeV Higgses. In Sect. 5 we discuss the implications of these results for a singlet scalar extension of the SM, and the possibility of exploring the nature of the EW phase transition in this scenario via direct scalar searches at CLIC. Finally we conclude in Sect. 6.

2 Heavy Higgs boson production at the compact linear collider

The three dominant processes contributing to Higgs boson production at a high-energy electron-positron collider are $e^+e^- \to HZ$, $e^+e^- \to H\nu\nu$ and $e^+e^- \to He^+e^-$ (see e.g. Fig. 1). Assuming a heavy scalar H with SM-like properties, we compute the production cross section[1] $\sigma_H^{\rm SM}$ as a function of the scalar mass m_H for each of the three processes and for $\sqrt{s} = 0.38$, 1.4, 3 TeV, shown in Fig. 2. We show both the case of unpolarized electron and positron beams (solid lines) and the possibility of using beam polarization, which can constitute a strong advantage in searching for new physics [12], assuming for definiteness an electron-positron beam polarization P_{e^-}, $P_{e^+} = -80\%, +30\%$ (dashed lines)[2] in the ballpark of the expected CLIC operation setup.

As highlighted in Fig. 2, the dominant Higgs production mechanism for both $\sqrt{s} = 1.4$ and 3 TeV is the vector boson fusion (VBF) process $e^+e^- \to H\nu\nu$. We also emphasize that the setup $\sqrt{s} = 380$ GeV does not allow to probe high values of m_H, and moreover it does not yield as many kinematical handles to disentangle the heavy scalar signal from SM backgrounds. In the rest of the paper we then focus on $e^+e^- \to H\nu\nu$ as Higgs production mechanism in CLIC, considering $\sqrt{s} = 1.4$ and 3 TeV as c.o.m. energies. The respective projected integrated luminosities we consider are $\mathcal{L} = 1500\,\text{fb}^{-1}$ and $2000\,\text{fb}^{-1}$ [6]. In all our subsequent analyses, we simulate CLIC production of the new scalar H via $e^+e^- \to H\nu\nu$ using MADGRAPH_AMC@NLO [13] with a subsequent decay into the relevant final state, and assuming electron and positron polarized beams with P_{e^-}, $P_{e^+} = -80\%, +30\%$ in all our analyses. We then shower/hadronise our events with PYTHIA 8.2 [14] and use DELPHES [15] for a simulation of the detector performance with the Delphes Tune for CLIC studies [16,17] (see also [18]).

Generically, we expect the production cross section for a heavy scalar H with mass m_H to be suppressed compared to that of a would-be SM Higgs of that mass, $\sigma_H^{\rm SM}$. This is e.g. the case of a singlet-like scalar which mixes with the SM Higgs, which we will discuss in detail in Sect. 5. However, in order to keep our analysis general, we will compute in the following the CLIC and LHC sensitivities to the production of a heavy "Higgs" H decaying respectively to a pair of EW gauge bosons VV (Sect. 3) and a pair of 125 GeV Higgs bosons hh

[1] For $e^+e^- \to He^+e^-$, the outgoing electrons are required to satisfy $|\eta| < 5$, $P_T > 5$ GeV.

[2] Here, -100% corresponds to a fully left-handed polarized beam and $+100\%$ to a fully right-handed polarized beam.

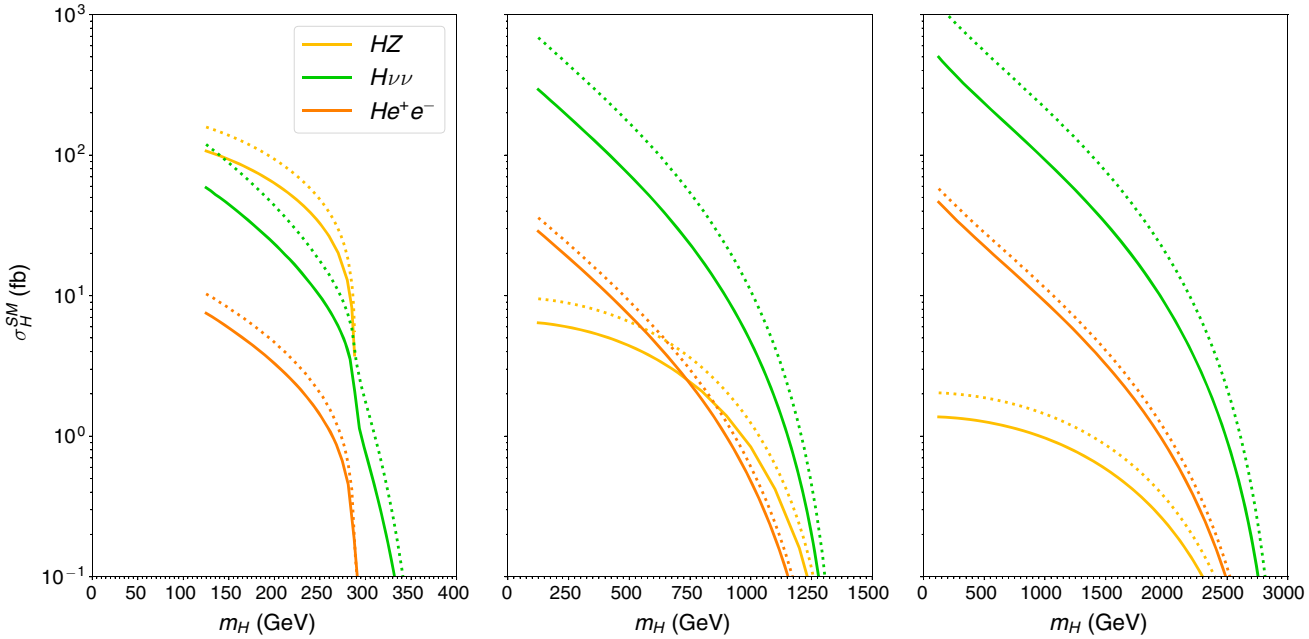

Fig. 2 Higgs production cross sections (assuming SM-like properties for H) $\sigma_H^{\rm SM}$ (in fb), as a function of m_H, for $\sqrt{s} = 380$ GeV (left), $\sqrt{s} = 1400$ GeV (middle) and $\sqrt{s} = 3000$ GeV (right), for unpolarized beams (solid) and $P_{e^-},\ P_{e^+} = -80\%,\ +30\%$ (dashed)

(Sect. 4), by considering the prospective model-independent bounds on the quantity $\kappa = \sigma_H/\sigma_H^{\rm SM}$, with σ_H the signal cross section for the respective channel, i.e., VV or hh.

3 Searching for heavy scalars in VV final states with $\sqrt{s} = 3$ TeV

We examine here the CLIC potential to search for new scalars via decays into EW gauge bosons $H \to VV$ ($V = W^{\pm}, Z$). We focus on leptonic final states $H \to 4\ell$ in Sect. 3.1 and $H \to 2\ell 2\nu$ in Sect. 3.2, and leave hadronic final states (requiring a more involved analysis, but being very promising due to the large branching fraction and the clean environment of CLIC) for a future analysis. We restrict our analysis to a CLIC c.o.m. energy $\sqrt{s} = 3$ TeV for our VV studies, as our results will show that the projected sensitivity for $\sqrt{s} = 1.4$ TeV would not be competitive with that of HL-LHC. In addition, for the $H \to 2\ell 2\nu$ final state analysis of Sect. 3.2, we focus on the $H \to W^+W^- \to 2\ell 2\nu$ signal decay channel: we have found that the projected sensitivity of this channel is significantly larger than the one that can be achieved for the $H \to ZZ \to 2\ell 2\nu$ signal channel, and thus disregard the latter in the following.

For both analyses in Sects. 3.1 and 3.2 we obtain present bounds (LHC) and future reach (HL-LHC and CLIC) for the signal strength $\kappa \equiv \sigma_H/\sigma_H^{\rm SM}$, i.e., the ratio of the signal cross section in the VV final state to its corresponding value assuming the SM (for a given m_H) for both the production cross section of H and its branching fraction $H \to VV$.

3.1 $H \to 4\ell$

The main SM backgrounds for heavy scalar production (in VBF) and subsequent decay $H \to ZZ \to 4\ell$ are the SM Higgs production $e^+e^- \to h\nu\nu$ ($h \to 4\ell$) and the EW processes $e^+e^- \to ZZ \to 4\ell$, $e^+e^- \to W^+W^-Z \to 4\ell 2\nu$, $e^+e^- \to ZZ\nu\nu$ ($ZZ \to 4\ell$). As initial event selection, we require four reconstructed leptons within the detector acceptance region ($|\eta_\ell| \leq 2.54$ for electrons and muons), yielding two same-flavour lepton pairs. In case of multiple possible pairings among the four leptons $\ell_{a,b,c,d}$ we choose the pairing minimising the function $\chi(m_{\ell_a\ell_b}, m_{\ell_c\ell_d})$

$$\chi = \sqrt{\frac{\left(m_{\ell_a\ell_b} - m_Z\right)^2}{\Delta m_Z^2} + \frac{\left(m_{\ell_c\ell_d} - m_Z\right)^2}{\Delta m_Z^2}} \tag{3.1}$$

with $m_Z = 91$ GeV and the choice $\Delta m_Z = 12$ GeV. We then select events for which $\chi < 1$, and define the signal region (SR) as the invariant mass window $m_{4\ell} \in [m_H - 15\,\text{GeV},\ m_H + 12\,\text{GeV}]$. We note that apart from the process $e^+e^- \to ZZ\nu\nu$ ($ZZ \to 4\ell$), the contribution of the SM backgrounds to the signal region is negligible[3]

[3] The SM Higgs and $e^+e^- \to W^+W^-Z$ backgrounds are strongly suppressed by the condition $\chi < 1$, while the $e^+e^- \to ZZ$ background

Table 1 3 TeV CLIC cross section (in fb) for signal (for $m_H = 300$, 600, 900 GeV respectively) and the dominant SM background $\sigma_B^{ZZ\nu\nu}$ at different stages in the event selection and in the signal region (SR) for $m_H = 300$, 600, 900 GeV respectively (see text for details)

$\sqrt{s} = 3$ TeV	σ_H^{300}	σ_H^{600}	σ_H^{900}	$\sigma_B^{ZZ\nu\nu}$
Event selection	0.711	0.388	0.107	0.303
$H \to 4\ell$ **selection**				
$\chi(m_{\ell_a\ell_b}, m_{\ell_c\ell_d}) < 1$	0.631	0.351	0.096	0.232
SR_{300}	0.621			0.017
SR_{600}		0.319		0.0053
SR_{900}			0.075	0.0016

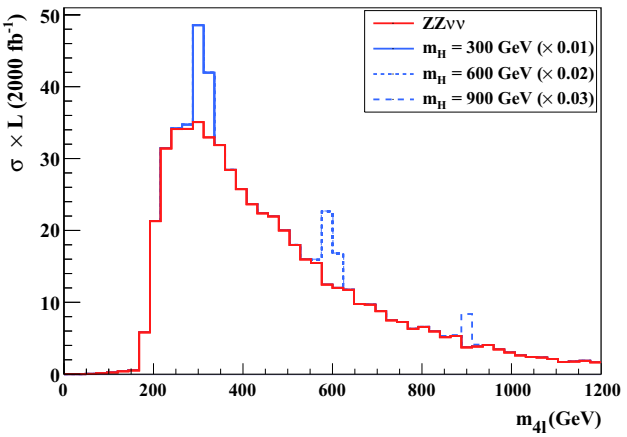

Fig. 3 $m_{4\ell}$ distribution (with the vertical axis corresponding to the number of events for an integrated luminosity $\mathcal{L} = 2000\,\text{fb}^{-1}$) for the signal $e^+e^- \to H\nu\nu$ ($H \to ZZ \to 4\ell$) with $m_H = 300$ GeV (solid blue), 600 GeV (dotted blue), 900 GeV (dashed blue) and the dominant SM background $e^+e^- \to ZZ\nu\nu$ ($ZZ \to 4\ell$) (red), for $\sqrt{s} = 3$ TeV CLIC

(less than one event expected for an integrated luminosity $\mathcal{L} = 2000$ fb). The cross section of the SM $e^+e^- \to ZZ\nu\nu$ ($ZZ \to 4\ell$) background and three benchmark signal scenarios ($m_H = 300$ GeV, 600 GeV, 900 GeV) at various stages in the selection process is shown in Table 1. We also show the $m_{4\ell}$ invariant mass distribution after event selection for the $ZZ\nu\nu$ SM background and the three benchmark signal scenarios in Fig. 3.

From the above analysis, we obtain the projected 95% C.L. sensitivity reach of $\sqrt{s} = 3$ TeV CLIC with $\mathcal{L} = 2000$ fb, in the mass range $m_H \in [200\,\text{GeV}, 1\,\text{TeV}]$. We perform a likelihood analysis based on the number of signal (s) and background (b) events in the signal region, the (Poisson) likelihood function given by

$$L(\kappa) = e^{-(\kappa\, s + b)}\, \frac{(\kappa\, s + b)^n}{n!} \tag{3.2}$$

Footnote 3 continued
is severely reduced by reconstructing the invariant mass $m_{4\ell}$ at values significantly away from $\sqrt{s} = 3$ TeV.

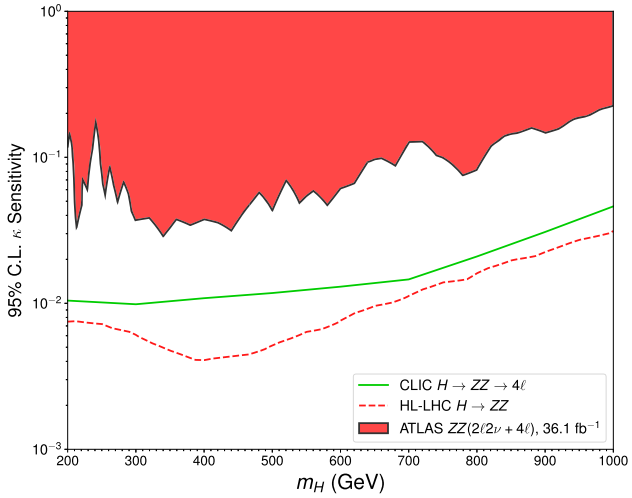

Fig. 4 95% C.L. sensitivity to $\kappa = \sigma_H/\sigma_H^{\text{SM}}$ as a function of m_H for $e^+e^- \to H\nu\nu$ ($H \to ZZ \to 4\ell$) at 3 TeV CLIC with $\mathcal{L} = 2000\,\text{fb}^{-1}$ (solid green line). Shown for comparison are the 95% C.L. excluded region from present ATLAS $H \to ZZ$ searches [19] (red region) and the projected HL-LHC (13 TeV, $\mathcal{L} = 3\,\text{ab}^{-1}$) expected 95% C.L. exclusion sensitivity (dashed red line)

with the number of observed events (n) assumed to match the background prediction ($n = b$), and $\kappa \equiv \sigma_H/\sigma_H^{\text{SM}}$ being the signal strength. We use the test statistic Q_κ

$$Q_\kappa \equiv -2\,\text{Log}\left[\frac{L(\kappa)}{L(0)}\right], \tag{3.3}$$

to obtain the 95% C.L. exclusion sensitivity, given by $Q_\kappa = 3.84$. This is shown in Fig. 4 (solid green line). For comparison, we show the present ($\sqrt{s} = 13$ TeV LHC with $\mathcal{L} = 36.1\,\text{fb}^{-1}$) limits on κ from ATLAS $H \to ZZ$ searches [19], with the SM (gluon fusion) production cross section for H obtained from [20]. We also show the HL-LHC ($\sqrt{s} = 13$ TeV with $\mathcal{L} = 3\,\text{ab}^{-1}$) projected 95% C.L. sensitivity from a naive $\sqrt{\mathcal{L}}$ scaling w.r.t. to the present expected exclusion sensitivity from [19]. As is apparent from Fig. 4, the sensitivity that can be achieved by CLIC in heavy scalar searches $H \to ZZ \to 4\ell$ is at best comparable to that of HL-LHC. However, we emphasize that while heavy scalar searches via leptonic final states are bound to yield the best sensitivity at the LHC, for CLIC it is expected that hadronic final states could surpass the sensitivity of leptonic ones, and a future study in this direction is well worth pursuing.

As a final remark on the analysis, we stress that for $m_H \gtrsim 1$ TeV the mean separation between the two leptons coming from each Z decay $\Delta R \sim 2m_Z/|\mathbf{P}_Z| \sim 4m_Z/m_H < 0.4$ and our analysis (which imposes a lepton isolation $\Delta R^{\text{min}} = 0.5$ from the DELPHES lepton reconstruction criteria) becomes highly inefficient. Gaining sensitivity to higher masses requires decreasing the required ΔR^{min} lepton isolation (as e.g. exemplified in [19]). Still, it will be shown in Sect. 5 that the relevant mass range to consider for

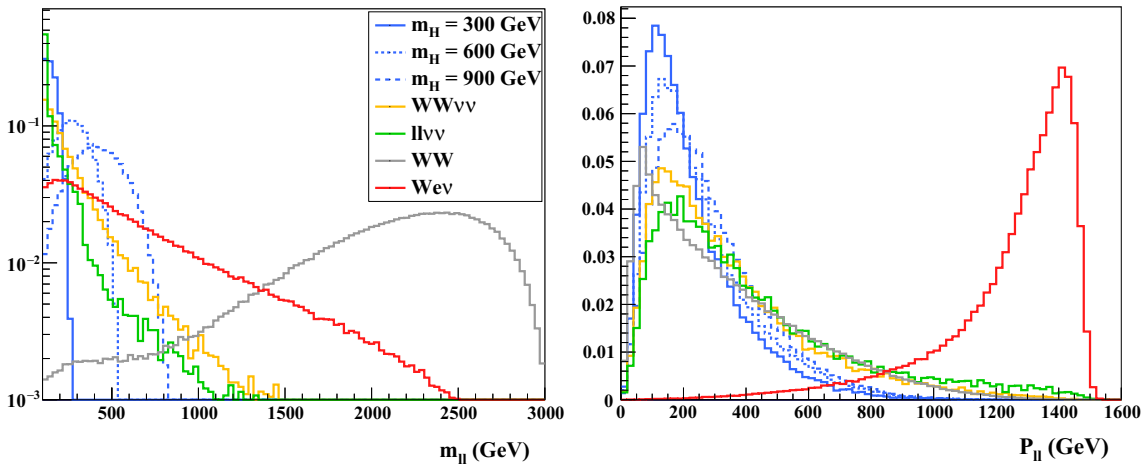

Fig. 5 Normalized kinematic distributions $m_{\ell\ell}$ (left) and $P_{\ell\ell}$ (right) for the signal $e^+e^- \to H\nu\nu$ ($H \to WW \to 2\ell 2\nu$) with $m_H = 300$ GeV (solid blue), 600 GeV (dotted blue), 900 GeV (dashed blue) and SM backgrounds $e^+e^- \to WW$ (grey), $e^+e^- \to e^{\pm}\nu W^{\mp}$ (red), $e^+e^- \to WW\nu\nu$ (yellow) and $e^+e^- \to \ell\ell\nu\nu$ (green), for $\sqrt{s} = 3$ TeV CLIC

the EW phase transition in the scenarios we will analyse is $m_H \lesssim 1$ TeV, and the lepton isolation criteria in our analysis are thus well-justified.

3.2 $H \to 2\ell\, 2\nu$

The relevant SM backgrounds for H production through $e^+e^- \to H\nu\nu$ and subsequent decay $H \to W^+W^- \to 2\ell\, 2\nu$ are:

(i) SM Higgs production through VBF: $e^+e^- \to h\,\nu\nu$ ($h \to 2\ell\, 2\nu$)
(ii) EW processes yielding a $2\ell\, 2\nu$ final state. These include $e^+e^- \to W^+W^-(\to 2\ell\, 2\nu)$, $e^+e^- \to ZZ\,(\to 2\ell\, 2\nu)$, $e^+e^- \to e^{\pm}\nu W^{\mp}\,(W^{\mp} \to \ell^{\mp}\nu)$, $e^+e^- \to Z\nu\nu\,(Z \to 2\ell)$, $e^+e^- \to Ze^+e^-(Z \to 2\nu)$ (in the last three processes, the states accompanying the produced $W^{\pm}$ or Z boson do not themselves come from a $W^{\pm}$ or Z boson).
(iii) The dominant EW processes yielding a $2\ell\, 4\nu$ final state: $e^+e^- \to W^+W^-\nu\nu\,(W^+W^- \to 2\ell\, 2\nu)$ and $e^+e^- \to ZZ\nu\nu\,(ZZ \to 2\ell\, 2\nu)$ (including the case where the initial neutrinos come from an on-shell Z boson).
(iv) We also include the process $e^+e^- \to \gamma\, 2\ell$ (including the case where the two leptons come from an on-shell Z boson).

For event selection we require two reconstructed leptons $\ell = e, \mu$ in the final state with $|\eta_\ell| \leq 2.44$. In addition, we require $m_{\ell\ell} \geq 100$ GeV to suppress backgrounds where the two leptons are coming from an on-shell Z boson, as well as the SM Higgs background. In order to subsequently suppress the SM backgrounds, we require $|\eta_\ell| \leq 1.5$ (the signal events feature rather central leptons, as opposed to several SM backgrounds) and $1 \leq \Delta R_{\ell\ell} \leq 3.5$. Finally, we also require $P_{\ell\ell} \leq 500$ GeV.

After the above selection cuts, the background from the SM Higgs becomes completely negligible. In addition, the $m_{\ell\ell}$ spectrum for the backgrounds $e^+e^- \to \gamma\, 2\ell$ and $e^+e^- \to Ze^+e^-(Z \to 2\nu)$ after the selection cuts features $m_{\ell\ell} \gtrsim 2$ TeV, which leads to a negligible overlap with the signal region domain (discussed below). In the following, we then consider as dominant backgrounds the processes $e^+e^- \to W^+W^-(\to 2\ell\, 2\nu)$, $e^+e^- \to e^{\pm}\nu W^{\mp}\,(W^{\mp} \to \ell^{\mp}\nu)$, $e^+e^- \to \ell\ell\,\nu\nu$ (with the final states not coming from W boson(s)) and $e^+e^- \to W^+W^-\nu\nu\,(W^+W^- \to 2\ell\, 2\nu)$. The (normalized) $m_{\ell\ell}$, $P_{\ell\ell}$, η_ℓ and $\Delta R_{\ell\ell}$ kinematic distributions after event selection and imposing $m_{\ell\ell} \geq 100$ GeV are shown in Figs. 5 and 6.
We define the signal region SR as:

$$\max(100\ \text{GeV},\ C - \Delta) \leq m_{\ell\ell} \leq C + \Delta,$$
$$\begin{cases} C(m_H) = 0.457 \times m_H - 15\,\text{GeV} \\ \Delta(m_H) = 0.264 \times m_H - 6.5\,\text{GeV} \end{cases} \tag{3.4}$$

which we obtain from an approximate fit to the m_H-dependence of the $m_{\ell\ell}$ distribution's peak (median) and width (1.5×variance) for our signal samples after the event and cut-flow selection discussed above. The cross sections for the relevant backgrounds and signal benchmarks with $m_H = 300$ GeV, 600 GeV, 900 GeV after event selection, the subsequent cut-flow and the final signal region selection are given in Table 2.

Assuming $\mathcal{L} = 2000\,\text{fb}^{-1}$, we show the projected 95% C.L. sensitivity reach of the $e^+e^- \to H\nu\nu$ ($H \to WW \to 2\ell 2\nu$) search at $\sqrt{s} = 3$ TeV CLIC in Fig. 7, following the likelihood analysis already employed in Sect. 3.1. We note the partial loss of sensitivity for $m_H < 300$ GeV, as the $m_{\ell\ell}$ distribution for the signal mainly lies under the Z-

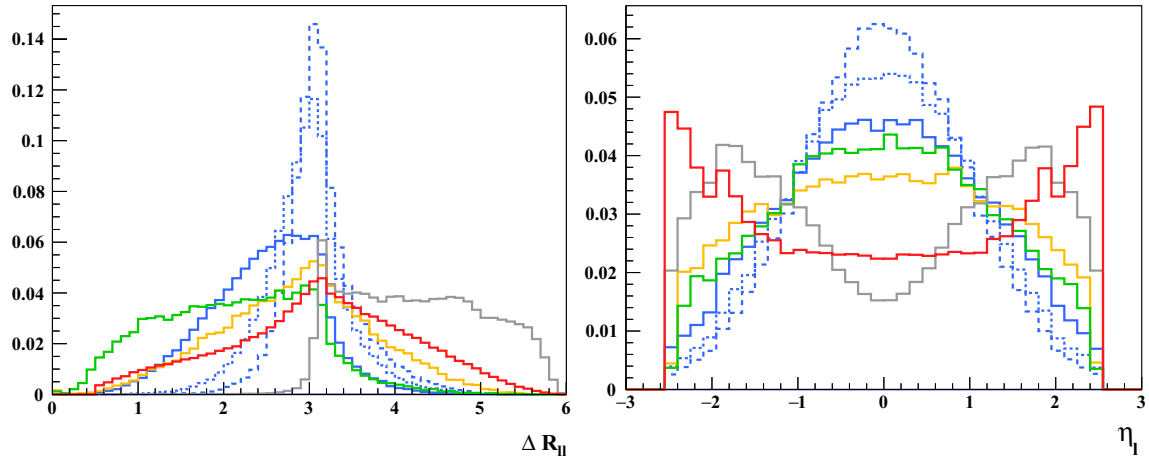

Fig. 6 Normalized kinematic distribution $\Delta R_{\ell\ell}$ (left) and η_ℓ (right) for the signal $e^+e^- \to H\nu\nu$ ($H \to WW \to 2\ell 2\nu$) with $m_H = 300$ GeV (solid blue), 600 GeV (dotted blue), 900 GeV (dashed blue) and SM backgrounds $e^+e^- \to WW$ (grey), $e^+e^- \to e^\pm\nu W^\mp$ (red), $e^+e^- \to WW\nu\nu$ (yellow) and $e^+e^- \to \ell\ell\nu\nu$ (green), for $\sqrt{s} = 3$ TeV CLIC

Table 2 3 TeV CLIC cross section (in fb) for signal (for $m_H = 300$, 600, 900 GeV respectively) and SM backgrounds σ_B^{WW}, σ_B^{Wev}, $\sigma_B^{\ell\ell\nu\nu}$, $\sigma_B^{WW\nu\nu}$ at different stages in the event, cut-flow and $H \to WW \to 2\ell\,2\nu$ signal region (SR) selection (see text for details)

$\sqrt{s} = 3$ TeV	σ_H^{300}	σ_H^{600}	σ_H^{900}	σ_B^{WW}	σ_B^{Wev}	$\sigma_B^{\ell\ell\nu\nu}$	$\sigma_B^{WW\nu\nu}$
Event selection	18.9	9.3	6.0	11.3	261	199	10.6
$H \to WW$ **selection**							
$m_{\ell\ell} \geq 100$ GeV	13.1	9.0	5.95	11.2	248	15.2	4.63
$\lvert\eta_\ell\rvert \leq 1.5$, $1 \leq \Delta R_{\ell\ell} \leq 3.5$	7.92	6.26	4.45	2.56	31.3	7.35	2.93
$P_{\ell\ell} \leq 500$ GeV	7.88	5.98	4.04	1.90	0.51	6.56	2.39
SR_{300}	6.90			0.043	0.138	4.79	1.32
SR_{600}		5.41		0.154	0.226	4.65	2.03
SR_{900}			3.57	0.229	0.152	2.19	1.28

peak of the $\ell\ell\nu\nu$ SM background, as can be inferred from Fig. 5. Figure 7 also shows the CLIC sensitivity reach in $\kappa = \sigma_H/\sigma_H^{\rm SM}$ from the combination of the $H \to WW \to 2\ell 2\nu$ and $H \to ZZ \to 4\ell$ (see Sect. 3.1) signal channels. For the sake of comparison, we show as well the present LHC limits for $H \to WW \to 2\ell 2\nu$ searches from ATLAS [21] ($\sqrt{s} = 13$ TeV LHC with $\mathcal{L} = 36.1\,\text{fb}^{-1}$), together with the projected 95% C.L. sensitivity reach in κ of ($\sqrt{s} = 13$ TeV) HL-LHC, which is essentially dominated by the $H \to ZZ$ searches (and thus corresponds to that shown in Fig. 4). Figure 7 highlights that $H \to VV$ searches at CLIC in the leptonic channels would reach a comparable sensitivity to that of HL-LHC.

4 Searching for heavy scalars in *hh* final states

We now turn to explore the CLIC sensitivity to new scalars through resonant di-Higgs signatures $H \to hh$. We focus on the $hh \to b\bar{b}b\bar{b}$ final state, which has the largest branching fraction while it does not suffer from the very large QCD background one has to face in the LHC environment [22,23]. We will show in the following that resonant di-Higgs searches at CLIC constitute a very sensitive probe of the existence of new scalars. In Sect. 4.1 we analyse the $\sqrt{s} = 3$ TeV CLIC prospects, and discuss those for $\sqrt{s} = 1.4$ TeV in Sect. 4.2.

4.1 $\sqrt{s} = 3$ TeV

The dominant backgrounds to the $e^+e^- \to H\nu\nu$ ($H \to hh \to 4b$) process at CLIC are from EW (including the SM non-resonant di-Higgs production contribution, on which we will comment in Sect. 5) and QCD processes yielding a $4b+2\nu$ final state. We reconstruct jets (within DELPHES) with FASTJET [24], using the Valencia clustering algorithm [25] (particularly well-suited for jet reconstruction in high energy e^+e^- colliders) in exclusive mode with $R = 0.7$ and $N = 4$ (number of jets). We perform our analysis for two different b-tagging working points within the CLIC Delphes Tune, corresponding respectively to a 70% and 90% b-tagging efficiency.[4] In each case, we select events with 4 b-tagged jets,

[4] For the 90% b-tagging working point, the background contribution from events with c-jets which are mis-identified as b-jets ceases to be negligible and should be considered in an exhaustive study. Nevertheless, the ratio of b-tagging efficiency to c-jet mistag rate is in this case

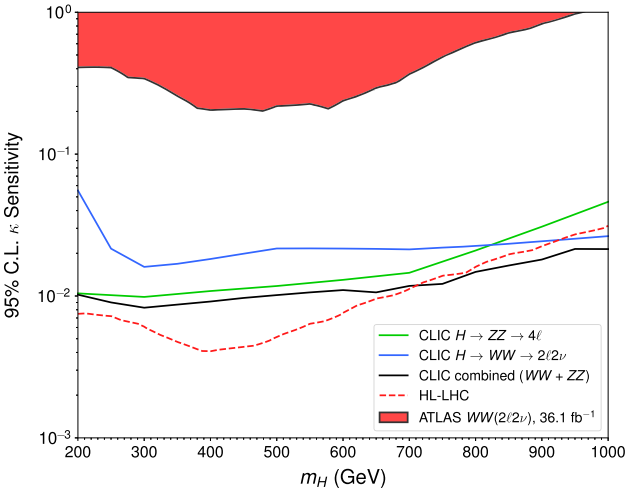

Fig. 7 95% C.L. sensitivity to $\kappa = \sigma_H/\sigma_H^{\rm SM}$ as a function of m_H for $e^+e^- \to H\nu\nu$ ($H \to WW \to 2\ell 2\nu$) at 3 TeV CLIC with $\mathcal{L} = 2000\,\text{fb}^{-1}$ (solid blue line), together with the sensitivity for $H \to ZZ \to 4\ell$ from Fig. 4 (solid green line) and the combined sensitivity (solid black line). Shown for comparison are the 95% C.L. excluded region from present ATLAS $H \to WW$ searches [21] (red region) and the projected HL-LHC (13 TeV, $\mathcal{L} = 3\,\text{ab}^{-1}$) 95% C.L. sensitivity reach (dashed red line), dominated by $H \to ZZ$ searches (see Sect. 3.1)

which are subsequently paired into two 125 GeV Higgs candidates by minimizing

$$\chi = \sqrt{\frac{\left(m_{b_1b_2} - \overline{m_h}\right)^2}{\Delta_h^2} + \frac{\left(m_{b_3b_4} - \overline{m_h}\right)^2}{\Delta_h^2}} \tag{4.1}$$

where $\overline{m_h} = 102$ GeV and $\Delta_h = 30$ GeV are obtained from an approximate fit to the signal simulation (we note that the average Higgs mass $\overline{m_h}$ is somewhat lower than the truth value $m_h = 125$ GeV as a result of the jet reconstruction process). We then select events with two SM Higgs candidates by requiring $\chi < 1$.

In Fig. 8 we show the signal efficiency after b-tagging and SM Higgs candidate selection (HH) as a function of m_H, together with the corresponding background (both EW and QCD) efficiencies (independent of m_H). After the SM Higgs candidate selection, the efficiency for the QCD background drops dramatically ($\sim 7 \times 10^{-5}$ for a 70% b-tagging efficiency and $\sim 2 \times 10^{-3}$ for a 90% b-tagging efficiency), such that the only relevant SM background is from the EW processes discussed above.

Footnote 4 continued
~ 0.2 (and backgrounds with mis-identified c-jets need to contain at least two of those), such that events with mis-identified jets are still subdominant, and we will not consider them here.

We define the Signal Region (SR) as

$$m_{4b} \in [C-\Delta, C+\Delta], \quad \begin{cases} C(m_H) = 0.96 \times m_H - 45\,\text{GeV} \\ \Delta(m_H) = 0.05 \times m_H + 40\,\text{GeV} \end{cases} \tag{4.2}$$

with both $C(m_H)$ and $\Delta(m_H)$ extracted from a fit to the signal simulation. The cross section of three benchmark signal scenarios ($m_H = 300$ GeV, 600 GeV, 900 GeV) and the SM backgrounds at various stages in the selection process is shown in Table 3-UP (for a b-tagging efficiency of 70%) and Table 3-DOWN (for a b-tagging efficiency of 90%).

From the above analysis, we obtain the projected 95% C.L. sensitivity reach of $\sqrt{s} = 3$ TeV CLIC ($\mathcal{L} = 2000$ fb) for $H \to hh \to b\bar{b}b\bar{b}$ in the mass range $m_H \in [300\,\text{GeV}, 1\,\text{TeV}]$ by performing a likelihood analysis, with a likelihood function and test statistic given respectively by (3.2) and (3.3). In contrast to the analysis from Sect. 3, here we define the signal strength κ as $\kappa \equiv \sigma_H/\sigma_H^{\rm SM} \times \text{BR}(H \to hh)$, with $\sigma_H/\sigma_H^{\rm SM}$ the ratio of the production cross section of H to its SM value (excluding the branching fraction into the corresponding final state). The results of this section are summarized in Fig. 9, and discussed in detail in the following Sect. 4.2 together with those obtained for $\sqrt{s} = 1.4$ TeV.

4.2 $\sqrt{s} = 1.4$ TeV

We now repeat the above analysis for a CLIC c.o.m. energy $\sqrt{s} = 1.4$ TeV with $\mathcal{L} = 1.5\,\text{ab}^{-1}$. The cross sections for the signal (for $m_H = 300$ GeV, 600 GeV, 900 GeV) and the SM backgrounds are shown in Table 4, with the signal region being defined as in the analysis from Sect. 4.1 and given by Eq. (4.2).

In Fig. 9 we show the corresponding sensitivity of CLIC with $\sqrt{s} = 1.4$ TeV (blue) and $\sqrt{s} = 3$ TeV (orange) for 70% b-tagging (solid) and 90% b-tagging (dashed) efficiencies, together with the present limits from CMS $H \to hh \to b\bar{b}b\bar{b}$ searches [26] with $\mathcal{L} = 35.9\,\text{fb}^{-1}$ (solid red) and the projected 95% C.L. sensitivity for HL-LHC with $\mathcal{L} = 3\,\text{ab}^{-1}$ (dashed red) based on a $\sqrt{\mathcal{L}}$ scaling w.r.t. to the present expected exclusion sensitivity from [26]. As Fig. 9 highlights, CLIC would greatly surpass the sensitivity of HL-LHC to resonant di-Higgs production: for a c.o.m. energy $\sqrt{s} = 1.4$ TeV the increase in sensitivity w.r.t. HL-LHC ranges from a factor $30 - 50$ for $m_2 \lesssim 400$ GeV, to roughly a factor 10 for $m_2 \sim 1$ TeV. For $\sqrt{s} = 3$ TeV the increase in sensitivity is a factor 50 or larger in the entire mass range $m_2 \in [250\,\text{GeV}, 1\,\text{TeV}]$, reaching two orders of magnitude sensitivity increase for $m_2 < 400$ GeV and $m_2 > 800$ GeV. At the same time, our results show that increasing the b-tagging efficiency above the 70% working point would benefit the reach of this search at CLIC

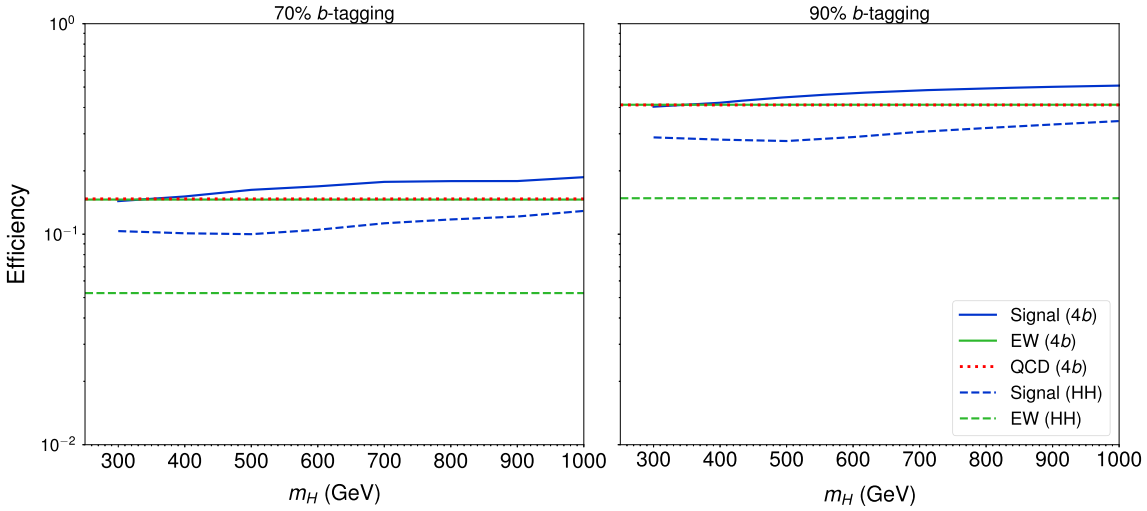

Fig. 8 Signal (blue), EW background (green) and QCD background (red) efficiency after b-tagging ($4b$, solid/dotted) and SM Higgs candidate selection (HH, dashed) as a function of m_H (see text for details)

Table 3 UP: 3 TeV CLIC cross section (in fb) for signal (for $m_H = 300, 600, 900$ GeV respectively) and SM backgrounds for a b-tagging efficiency of 70%, at different stages in the event selection and in the signal region (SR) for $m_H = 300, 600, 900$ GeV respectively (see text for details). DOWN: Same as above, for a b-tagging efficiency of 90%

$\sqrt{s} = 3$ TeV	σ_H^{300}	σ_H^{600}	σ_H^{900}	σ_B^{EW}	σ_B^{QCD}
Event selection (70% b-tagging)	12.85	8.52	5.19	0.407	0.048
$H \to hh$ **selection**					
$\chi(m_{b_1b_2}, m_{b_3b_4}) < 1$	9.26	5.29	3.52	0.146	$< 10^{-3}$
SR_{300}	8.99			0.0444	–
SR_{600}		4.80		0.0236	–
SR_{900}			3.03	0.0098	–
Event selection (90% b-tagging)	36.09	23.58	14.56	1.14	0.136
$H \to hh$ **selection**					
$\chi(m_{b_1b_2}, m_{b_3b_4}) < 1$	25.80	14.60	9.64	0.413	$< 10^{-3}$
SR_{300}	25.01			0.126	–
SR_{600}		13.32		0.063	–
SR_{900}			8.25	0.028	–

substantially. In our work we specifically explore a 90% working point, but a less extreme increase of the b-tagging efficiency would display a comparable associated sensitivity increase.

Altogether, the results of this section show that resonant di-Higgs production searches are a prominent and very sensitive probe of heavier Higgs bosons with CLIC. In the remainder of this work, we explore the sensitivity of these searches to the existence of a new singlet-like scalar interacting with the SM Higgs, and the implications for the properties of the EW phase transition in the early Universe.

5 Singlet scalar extension of the standard model

The (real) singlet extension of the SM is a simple scenario that can capture the phenomenology of the Higgs sector in more complete theories beyond the SM (like the NMSSM and Twin Higgs). At the same time, it constitutes a paradigm for achieving a strongly first order EW phase transition that could generate the observed matter-antimatter asymmetry of the Universe. The phenomenology of the SM extended by a real scalar singlet S (SM + S) has been widely studied in the literature (see e.g. [7–9,27–37]), including the connection to the EW phase transition [7,9,27,28,33,34,36] (see also [38,39]). We analyse here the sensitivity of CLIC to the parameter space leading to a first order EW phase transition by casting the results from the previous sections in terms of the SM + S scenario. We also explore the complementarity of CLIC with other probes of the EW phase transition – favoured parameter space in this scenario from HL-LHC and future colliders such as *FCC-ee* [34,36].

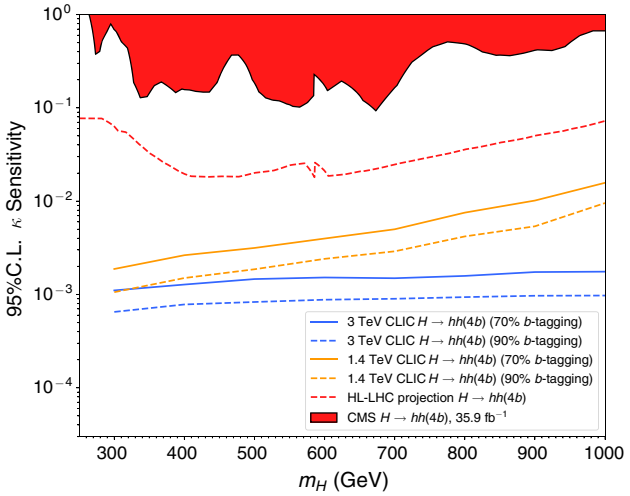

Fig. 9 CLIC 95% C.L. sensitivity to $\kappa = \sigma_H/\sigma_H^{\rm SM} \times {\rm BR}(H \to hh)$ as a function of m_H for $e^+e^- \to H\nu\nu\,(H \to hh \to 4b)$ at $\sqrt{s} = 1.4$ TeV with $\mathcal{L} = 1500\,{\rm fb}^{-1}$ (orange) and $\sqrt{s} = 3$ TeV with $\mathcal{L} = 2000\,{\rm fb}^{-1}$ (blue). In both cases the solid line corresponds to a 70% b-tagging efficiency and the dashed line to a 90% b-tagging efficiency. Shown for comparison are the LHC 95% C.L. excluded region from present CMS $H \to hh \to 4b$ searches [26] (red region) and the projected HL-LHC (13 TeV, $\mathcal{L} = 3\,{\rm ab}^{-1}$) expected 95% C.L. exclusion sensitivity (dashed red line)

5.1 Model and theoretical constraints

We consider the most general form for the SM + S scalar potential that depends on a Higgs doublet Φ and real singlet S (see e.g. [7,9]):

$$V(\Phi, S) = -\mu^2\left(\Phi^\dagger\Phi\right) + \lambda\left(\Phi^\dagger\Phi\right)^2 + \frac{a_1}{2}\left(\Phi^\dagger\Phi\right)S + \frac{a_2}{2}\left(\Phi^\dagger\Phi\right)S^2 + b_1 S + \frac{b_2}{2}S^2 + \frac{b_3}{3}S^3 + \frac{b_4}{4}S^4. \tag{5.1}$$

Upon EW symmetry breaking, $\Phi \to (v+h)/\sqrt{2}$ with $v = 246$ GeV. We note that a shift in the singlet field $S + \delta S$ does not lead to any change in the physics, which may be used to choose a vanishing vev for the singlet field in the EW broken minimum by requiring $b_1 = -a_1 v^2/4$. This is the choice we adopt in the following. Once the EW symmetry is broken, the singlet S and the SM Higgs h mix in the presence of a_1, yielding two mass eigestates h_1, h_2. We identify h_1 with the 125 GeV Higgs boson, and h_2 with the heavy state H discussed in the previous sections. The masses $m_1 = 125$ GeV, m_2 and the singlet-doublet mixing angle θ are related to the scalar potential parameters as

$$\begin{aligned} a_1 &= \frac{m_1^2 - m_2^2}{v}\, 2\sin\theta\cos\theta \\ b_2 + \frac{a_2\, v^2}{2} &= m_1^2\sin^2\theta + m_2^2\cos^2\theta \\ \lambda &= \frac{m_1^2\cos^2\theta + m_2^2\sin^2\theta}{2\,v^2} \end{aligned} \tag{5.2}$$

with $\mu^2 = \lambda\, v^2$. In the following we consider as independent parameters for our analysis the set $\{v,\ m_1,\ m_2,\ \theta,\ a_2,\ b_3,\ b_4\}$.

In order to obtain a viable SM + S scenario, we need to satisfy several theoretical constraints which we discuss below:

- *(Perturbative) unitarity and perturbativity* The size of the quartic scalar couplings in Eq. (5.1) is constrained by perturbative unitarity of the partial wave expansion of scattering amplitudes. The bound $|a_0| \leq 0.5$ for the leading order term in the partial wave expansion of the $h_2h_2 \to h_2h_2$ scattering amplitude, $a_0(h_2h_2 \to h_2h_2) = 3b_4/(8\pi)$, yields $b_4 < 4\pi/3$ (see e.g. [37]). In addition, we require perturbative values for a_2 and b_3/v: $|a_2| < 4\pi$, $|b_3|/v < 4\pi$.

Table 4 UP: 1.4 TeV CLIC cross section (in fb) for signal (for $m_H = 300$, 600, 900 GeV respectively) and SM backgrounds for a b-tagging efficiency of 70%, at different stages in the event selection and in the signal region (SR) for $m_H = 300$, 600, 900 GeV respectively (see text for details). DOWN: Same as above, for a b-tagging efficiency of 90%

$\sqrt{s} = 1.4$ TeV	σ_H^{300}	σ_H^{600}	σ_H^{900}	σ_B^{EW}	σ_B^{QCD}
Event selection (70% b-tagging)	6.18	2.17	0.456	0.140	0.039
$H \to hh$ **selection**					
$\chi(m_{b_1b_2}, m_{b_3b_4}) < 1$	4.61	1.36	0.306	0.052	$< 10^{-3}$
SR_{300}	4.50			0.022	–
SR_{600}		1.24		0.0068	–
SR_{900}			0.263	0.0014	–
Event selection (90% b-tagging)	17.25	5.88	1.26	0.385	0.108
$H \to hh$ **selection**					
$\chi(m_{b_1b_2}, m_{b_3b_4}) < 1$	12.85	3.64	0.843	0.143	$< 10^{-3}$
SR_{300}	12.51			0.059	–
SR_{600}		3.32		0.018	–
SR_{900}			0.725	0.0042	–

- *Boundedness from below of scalar potential* We require the absence of runaway directions in the scalar potential (5.1) at large field values. Along the h and S directions, this leads respectively to the bounds $\lambda > 0$ and $b_4 > 0$. For $a_2 < 0$ we further require $a_2 > -2\sqrt{\lambda\, b_4}$ to ensure boundedness from below along an arbitrary field direction.
- *Absolute stability of EW vacuum* First, the EW vacuum $(\langle h\rangle, \langle S\rangle) = (v, 0)$ must be a minimum. On one hand, this requires $b_2 > 0$, which by virtue of (5.2) yields an upper bound on the value of a_2

$$a_2 < \frac{2}{v^2}(m_1^2 \sin^2\theta + m_2^2 \cos^2\theta)\,. \tag{5.3}$$

On the other hand, for $(v, 0)$ to be a minimum the determinant of the scalar squared-mass matrix has to be positive

$$\begin{aligned}&\text{Det}\begin{pmatrix} \partial^2 V/\partial h^2 & \partial^2 V/\partial h \partial S \\ \partial^2 V/\partial h \partial S & \partial^2 V/\partial S^2 \end{pmatrix}\Bigg|_{(v,0)} \\ &\equiv \text{Det}\mathcal{M}_S^2 = 2\lambda v^2 b_2 - \frac{a_1^2 v^2}{4} > 0\,. \end{aligned}\tag{5.4}$$

In addition, we require that the EW vacuum is the absolute minimum of the potential. The conditions for this are discussed in detail in [9], and we summarise them here. It will prove convenient to define the quantities

$$\begin{aligned}\bar{\lambda}^2 &\equiv \lambda\, b_4 - \frac{a_2^2}{4} \\ m_* &\equiv \frac{\lambda\, b_3}{3} - \frac{a_2\, a_1}{8} \end{aligned}\tag{5.5}$$

$$\mathcal{D}^2(S) \equiv v^2\left(1 - \frac{a_1\, S}{2\lambda v^2} - \frac{a_2\, S^2}{2\lambda v^2}\right) \tag{5.6}$$

with $h^2 = \mathcal{D}^2(S)$ corresponding to the minimization condition $\partial V/\partial h = 0$ for values $h \neq 0$. From the analysis of [9], we immediately find that a sufficient (though not necessary) condition for the EW vacuum to be the absolute minimum of V is given by

$$\bar{\lambda}^2 > \frac{m_*^2\, v^2}{16\,\text{Det}\mathcal{M}_S^2}\,. \tag{5.7}$$

When (5.7) is not satisfied, there exists for $\bar{\lambda}^2 > 0$ a minimum $S = \omega$ along $\mathcal{D}^2(S)$ which is deeper than the EW vacuum, and in order for the EW vacuum to still be the absolute minimum of V, it is necessary that $\mathcal{D}^2(\omega) < 0$ (in order for this new minimum to be unphysical). In addition, in this case we also need to require that no new minimum exists along the $h = 0$ field direction which is deeper than the EW one. The extrema along this direction are given by the real solutions of the equation

$$b_4 S^3 + b_3 S^2 + b_2 S + b_1 = 0\,. \tag{5.8}$$

Finally, when $\bar{\lambda}^2 < 0$ a necessary and sufficient condition for the EW vacuum to be the absolute minimum of V is the absence of a deeper minimum along the $h = 0$ field direction, which we have just discussed above.

In Figs. 10, 11 and 12, we show, for fixed values of $m_2 =$ 300 GeV, 500 GeV, 700 GeV and $\sin\theta = 0.1, 0.05$, the points that satisfy the above requirements in the plane a_2, b_3/v, with the parameter b_4 being scanned over. We find that, for a given choice of $(a_2, b_3/v)$, the requirements are generically satisfied more robustly as b_4 increases,[5] and as such we demand that there is a value of $b_4 \in [0, 4\pi/3]$ above which the EW vacuum is the absolute minimum of the potential.

Before moving on to the next section, we note that for large values of a_2 and b_3 the 1-loop corrections may become important and might allow for new regions that fulfill the above stability/unitarity/perturbativity conditions (see the discussion in [36]), particularly for low values of m_2, for which such regions with large a_2 and/or b_3 do no satisfy these requirements at tree-level (see Figs. 10, 11, 12). We leave an investigation of the impact of 1-loop corrections on the above theoretical constraints for the future. We also note that, as compared to [36], our analysis has a smaller range of allowed values for b_4 which is partially responsible (together with the different chosen range for m_2) for the different shape of the tree-level allowed region.

5.2 EW phase transition in the SM + S

The EW symmetry is (generally) restored at high temperatures $T \gg v$. EW symmetry breaking then occurs when the temperature of the Universe drops due to expansion, and it becomes energetically favorable for the Higgs field Φ to acquire a non-zero expectation value $\varphi_h = v_T \neq 0$. When there exists a potential barrier separating the symmetric vacuum $\varphi_h = 0$ from the broken one v_T, the EW phase transition is of first order. The temperature at which the two vacua become degenerate in energy is known as the critical temperature T_c, and the EW phase transition is considered to be strongly first order if[6] $v_T(T_c)/T_c \gtrsim 1$.

[5] This is true except in certain regions of $a_2 < 0$, where "islands of stability" in the parameter b_4 exist (that is, a very narrow range of b_4 within $[0, 4\pi/3]$ where the EW vacuum is the absolute minimum of the potential. These regions are however not relevant for the subsequent EW phase transition discussion, and we disregard them in the following.

[6] A more accurate criterion can be obtained by considering the "nucleation" temperature T_n at which the phase transition actually takes place,

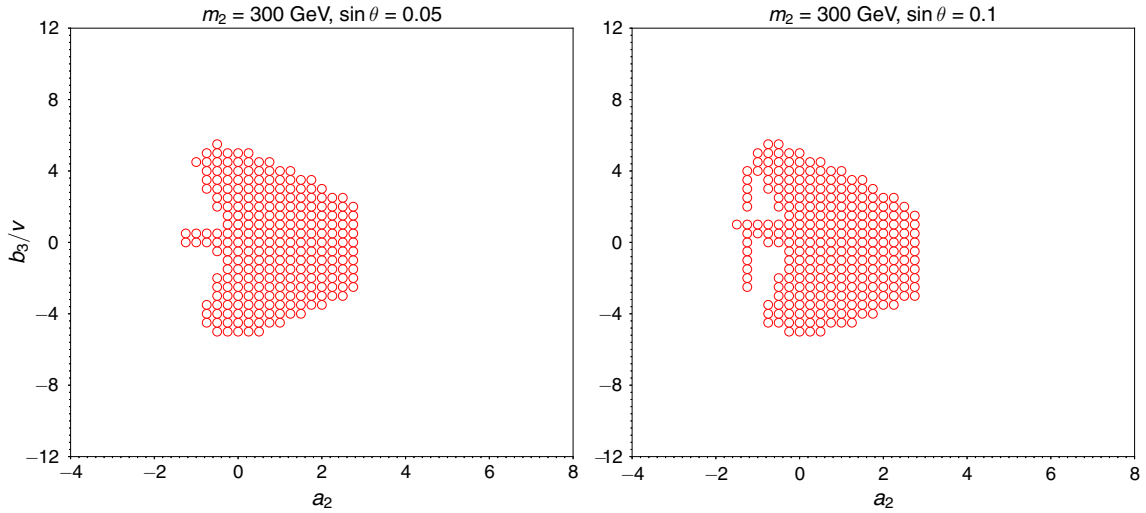

Fig. 10 Region of parameter space in $(a_2, b_3/v)$ and fixed $m_2 = 300$ GeV and $\sin\theta = 0.05$ (left), $\sin\theta = 0.1$ (right), compatible with the requirements of unitary, perturbativity and absolute stability of the EW vacuum. The parameter b_4 has been scanned over (see text for details)

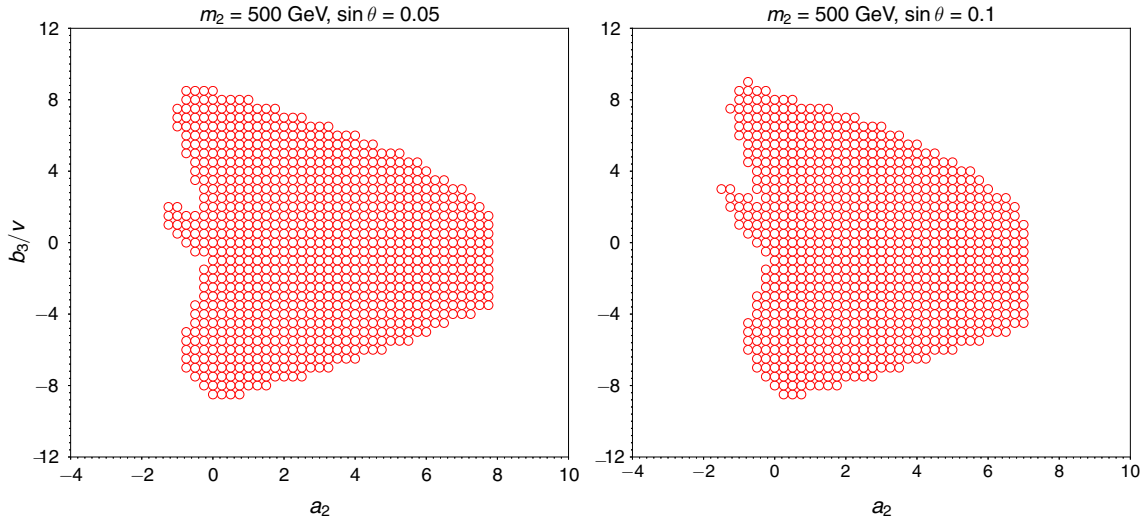

Fig. 11 Same as Fig. 10, but for $m_2 = 500$ GeV

For the analysis of the EW phase transition in the SM + S scenario, we adopt in the following a conservative strategy: It is known that including the 1-loop $T = 0$ (Coleman-Weinberg) contributions to the effective potential introduces a gauge-dependence[7] in the evaluation of various phase transition parameters, such as T_c [40–42]. However for a singlet-driven first order EW phase transition as in the SM + S, the properties of the transition are dominantly determined by tree-level effects. It is then possible in a first approximation to perform the analysis of the phase transition using the tree-level potential (5.1) augmented by the T^2 terms from the high-T expansion of the finite-temperature effective potential (see e.g. [9]):

$$V_{T^2} = \left(\frac{c_h}{2}h^2 + \frac{c_s}{2}S^2 + c_t S\right)T^2\,, \tag{5.9}$$

where

$$c_h = \frac{1}{48}\left(9g^2 + 3g'^2 + 12y_t^2 + 24\lambda + 2a_2\right)$$

$$c_s = \frac{1}{12}\left(2a_2 + 3b_4\right)$$

$$c_t = \frac{1}{12}\left(a_1 + b_3\right)$$

Footnote 6 continued
and requiring $v_T(T_n)/T_n \gtrsim 1$. It is nevertheless a reasonable approximation in general to consider $v_T(T_c)/T_c \gtrsim 1$ instead.

[7] This gauge-dependence arises from the Goldstone and gauge boson contribution to the Coleman–Weinberg potential, as well as to the cubic term of the finite-temperature potential in the high-T expansion (see [40] for a detailed discussion).

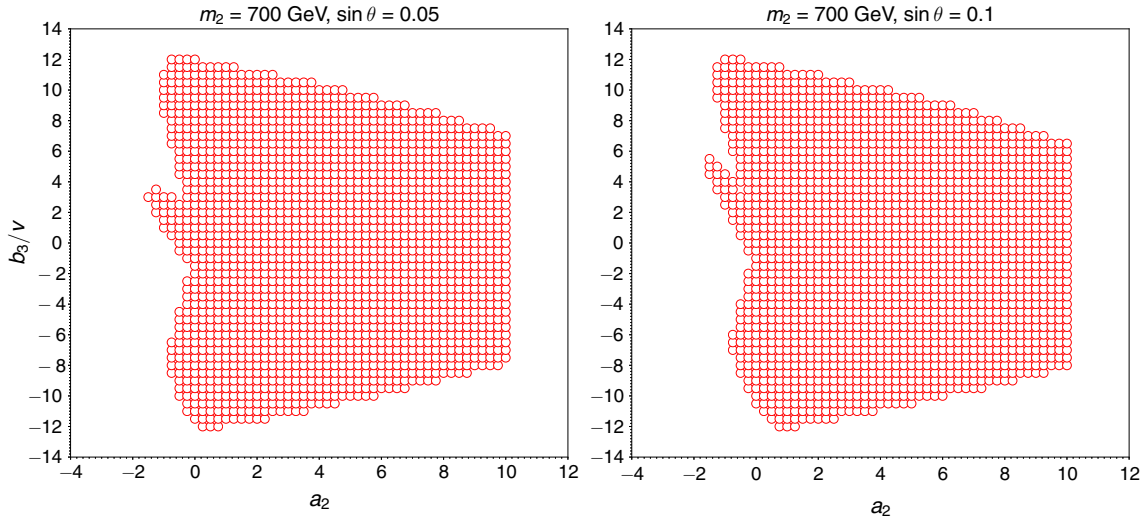

Fig. 12 Same as Fig. 10, but for $m_2 = 700$ GeV

as these are manifestly gauge invariant.[8] This approach, which we take in the present work, nevertheless disregards 1-loop terms that could be numerically important in certain regions of parameter space, particularly for large values of a_2 and/or b_3, strengthening the phase transition in those regions. We believe the choice made here then provides a conservative prediction for a strongly first order EW phase transition.

In the following we use the numerical programme CosmoTransitions [43] (v2.0.2) to find the points in parameter space with a viable strongly first order EW phase transition, for fixed values of m_2 and $\sin\theta$ while scanning over a_2, b_3 and b_4. Specifically, for each scan point we evolve the effective potential [combining (5.1) and (5.9)] from $T = 0$ up and look for coexisting and degenerate phases at some temperature(s) $T_i^* = T_c$. We consider the point to have a strongly first order EW phase transition when at (any) such temperature there is coexistence of a phase with $\varphi_h = 0$ (irrespectively of the singlet vacuum expectation value) and a phase with $\varphi_h = v_T$, separated by a potential barrier and such that $v_T/T_c > 1$. The results of our EW phase transition scan are shown in Figs. 15, 16 and 17, with the same stability/unitarity/perturbativity requirements as in Figs. 10, 11 and 12. Our EW phase transition scan shows that, as the mass m_2 increases, the values of a_2 and b_3/v required to achieve a strongly first order transition also increase substantially, approaching the perturbativity limit (particularly for a_2) for $m_2 \sim 700 - 800$ GeV. This yields a clear target reach for high-energy colliders regarding a singlet-driven EW phase transition.[9]

In the next section, we study the sensitivity to the parameter space of the SM + S scenario that can be achieved at CLIC and compare it to the corresponding sensitivity achievable at HL-LHC and *FCC-ee*. We pay particular attention to the parameter space region where a strongly first order EW phase transition would be achieved, and discuss the interplay of direct probes (searches for the singlet-like scalar) and indirect probes (e.g. deviations of the couplings of the 125 GeV Higgs w.r.t. its SM values) in this sense.

5.3 CLIC sensitivity to the SM + S: probing the EW phase transition

We analyse here the CLIC prospects for probing the parameter space leading to a strongly first order EW phase transition in the SM + S scenario, based on the results from the previous sections. In addition, we discuss the complementarity with probes of this parameter space via other possible future colliders, such as *FCC-ee* [34], as well as from the HL-LHC.

Let us start by pointing out that due to the singlet-doublet mixing, the couplings of h_1 (h_2) to SM gauge bosons and fermions are universally rescaled w.r.t. the corresponding SM Higgs coupling values by $\cos\theta$ ($\sin\theta$). In addition to these, the tri-scalar interactions play an important role in the discussion of both di-Higgs production at colliders and the nature of the EW phase transition. Specifically, we focus on the interactions $\lambda_{211} h_2 h_1 h_1$ and $\lambda_{111} h_1 h_1 h_1$, which follow from (5.1) after EWSB, with

[8] The last term in (5.9) is gauge invariant at 1-loop, but not necessarily at higher loop order [28,36]. Still, we choose here to keep it in the analysis (in contrast to [28,36], where such term is discarded).

[9] We emphasize again that the 1-loop Coleman–Weinberg and finite-T terms of the effective potential disregarded here will have some impact on the precise shape of the parameter space region yielding a strongly first order EW phase transition, and the value of m_2 above which such a strong transition stops being feasible. Yet, the bound $m_2 \lesssim 700 - 800$ GeV will not be significantly modified.

$$\lambda_{211} = \frac{1}{4}\Big[a_1\, c_\theta^3 + 4v(a_2 - 3\lambda)\, c_\theta^2 s_\theta - 2(a_1 - 2\,b_3)\, c_\theta s_\theta^2 - 2a_2 v\, s_\theta^3\Big]$$
$$\lambda_{111} = \lambda v\, c_\theta^3 + \frac{1}{4}a_1\, c_\theta^2 s_\theta + \frac{1}{2}a_2\, v\, c_\theta s_\theta^2 + \frac{b_3}{3}s_\theta^3 \qquad (5.10)$$

with $c_\theta \equiv \cos\theta$ and $s_\theta \equiv \sin\theta$. The coupling λ_{211} controls the partial width of the decay $h_2 \to h_1 h_1$ for $m_2 > 250$ GeV, given by

$$\Gamma_{h_2\to h_1 h_1} = \frac{\lambda_{211}^2\sqrt{1 - 4\,m_1^2/m_2^2}}{8\pi m_2}\,. \qquad (5.11)$$

Denoting by $\Gamma^{\rm SM}(m_2)$ the total width of a SM-like Higgs with mass m_2 (as given e.g. in [20]), the branching fraction $\mathrm{BR}(h_2 \to h_1 h_1)$ is simply given by

$$\mathrm{BR}(h_2 \to h_1 h_1) = \frac{\Gamma_{h_2\to h_1 h_1}}{\sin^2\theta\ \Gamma^{\rm SM}(m_2) + \Gamma_{h_2\to h_1 h_1}}\,. \qquad (5.12)$$

In the limit of high m_2 masses, this branching fraction is expected to be fixed by the Equivalence Theorem,[10] $\mathrm{BR}(h_2 \to h_1 h_1) \simeq 0.25$, but different values of a_2 and b_3 can lead to some departure from this expectation. We show in Fig. 13 the values of $\mathrm{BR}(h_2 \to h_1 h_1)$ for $m_2 = 500,\ 700$ GeV and $\sin\theta = 0.05$ for illustration. At the same time, the production cross section for h_2 normalized to the SM value (for a given mass m_2) takes in the case of the SM + S scenario the very simple form $\sigma_H/\sigma_H^{\rm SM} = \sin^2\theta$, due to the universal rescaling discussed above.

With all these ingredients, we can readily interpret both the HL-LHC and CLIC sensitivities to the parameter space of the SM + S scenario from direct searches of the singlet-like scalar h_2, as discussed in Sects. 3 and 4. In addition to these direct searches, we consider here two indirect collider probes of the SM + S scenario:

(i) The measurement of the 125 GeV Higgs self-coupling λ_{111}. The projected sensitivity to the Higgs self-coupling at CLIC, combining the $\sqrt{1.4}$ TeV and $\sqrt{3}$ TeV runs is $\delta\lambda_{111} \equiv \left|\lambda_{111}^{\rm SM+S} - \lambda_{111}^{\rm SM}\right|/\lambda_{111}^{\rm SM} = 19\%$ (for a choice of beam polarization similar to the one considered in this work) [44], with $\lambda_{111}^{\rm SM} = \lambda\, v = 31.8$ GeV being the self-coupling value in the SM. For the Higgs self-coupling in the SM + S scenario, we consider both the tree-level contribution from (5.10) and the 1-loop contribution computed to order $\sin\theta$ and given by [36] (note the different λ_{111} normalization in our work w.r.t. [36]):

$$\Delta\lambda_{111}^{1-\rm loop} = \frac{1}{16\pi^2}\left(\frac{a_2^3\, v^3}{12\, m_2^2} + \frac{a_2^2\, b_3\, v^2}{2\, m_2^2}\sin\theta\right)\,. \qquad (5.13)$$

We nevertheless stress that it is not at all clear that the information on $\lambda_{111}^{\rm SM+S}$ from the non-resonant di-Higgs signal can be extracted from the data independently from the resonant di-Higgs contribution. In particular, since the non-resonant Higgs pair invariant mass distribution m_{hh} peaks around 300–400 GeV (see [45]), for masses $m_2 \lesssim 500$ GeV disentangling the two contributions might be challenging.

(ii) The measurement of the Higgs associated production cross section σ_{Zh} at CLIC and *FCC-ee*. At CLIC, the expected precision in the determination of the associated production cross section for the 125 GeV Higgs is $\delta\sigma_{Zh} \equiv \left|\sigma_{Zh} - \sigma_{Zh}^{\rm SM}\right|/\sigma_{Zh}^{\rm SM} = 1.65\%$ [44].[11] A future circular e^+e^- collider like *FCC-ee* could reach a precision $\delta\sigma_{Zh} = 0.4\%$ [47,48]. For a small singlet-doublet mixing (as we are considering here), the deviation in the Higgs production cross section w.r.t. its SM value $\delta\sigma_h$ (corresponding here also to $\delta\sigma_{Zh}$) is approximately given by (see e.g. [34,36,49]):

$$\delta\sigma_h = \left|-\sin^2\theta + \frac{\lambda_{221}^2}{16\,\pi^2\, m_1^2}(1 - F(\tau))\right|\,, \qquad (5.14)$$

where the first term is just the tree-level deviation and the second term corresponds to the leading 1-loop correction, with $\tau = m_1^2/(4m_2^2)$ and $F(\tau)$, λ_{221} given by

$$F(\tau) = \frac{\mathrm{Arcsin}(\sqrt{\tau})}{\sqrt{\tau(1-\tau)}}\,, \qquad (5.15)$$
$$\lambda_{221} = \frac{1}{2}\,a_2\, v\, c_\theta^3 + \left(b_3 - \frac{a_1}{2}\right) c_\theta^2 s_\theta + v(3\lambda - a_2)\, c_\theta s_\theta^2 + \frac{a_1}{4}\, s_\theta^3\,. \qquad (5.16)$$

As a comparison, the projected HL-LHC precision in $\delta\sigma_h$ from a global fit to the measured 125 GeV Higgs signal strengths is [50] $\delta\sigma_h \simeq 3\%$ (assuming negligible theory uncertainties; taking into account the present theory uncertainties the projected value is $\delta\sigma_h \simeq 6\%$).

In Fig. 14 we show the CLIC sensitivity to the SM + S scenario in the plane (m_2, $\sin\theta$) from direct searches of the scalar h_2 assuming for concreteness a branching fraction $\mathrm{BR}(h_2 \to h_1 h_1) = 0.25$ (as naively expected from the Equivalence Theorem) and a 90% b-tagging efficiency. We also show the current and projected LHC bounds from direct searches of h_2 in the VV channel and measurements

[10] We are indebted to Andrea Tesi for reminding us of this.

[11] It has been recently highlighted that the CLIC sensitivity to a deviation in the Higgs production cross section in VBF w.r.t. its SM value is $\delta\sigma_h \sim 0.2\% - 0.4\%$ [46], similar to the expected sensitivity of *FCC-ee* to $\delta\sigma_{Zh}$.

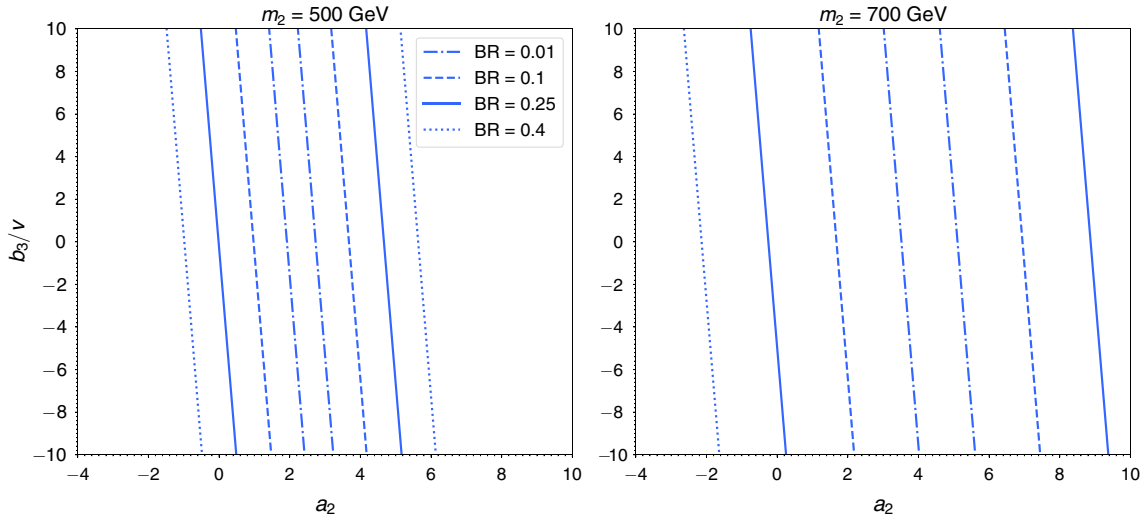

Fig. 13 Branching fraction BR($h_2 \to h_1 h_1$) values in the SM + S scenario for $\sin\theta = 0.05$ and $m_2 = 500$ GeV (left), $m_2 = 700$ GeV (right) in the plane (a_2, b_3/v)

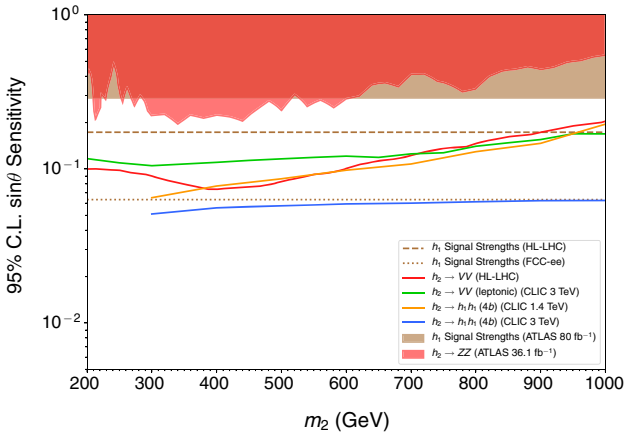

Fig. 14 95% C.L. bounds in the (m_2, sinθ) from current LHC (ATLAS, 80 fb^{-1}) Higgs signal strength measurements [51] (brown region), and $h_2 \to VV$ searches [19] (red region), together with future HL-LHC (dashed brown) and *FCC-ee* (dotted brown) sensitivity from Higgs signal strength measurements, as well as 1.4 and 3 TeV CLIC 95% C.L. sensitivities from $h_2 \to h_1 h_1$ ($4b$), as well as HL-LHC and 3 TeV CLIC sensitivities from $h_2 \to VV$, shown respectively as orange, blue, red and green lines. All direct searches assume BR($h_2 \to h_1 h_1$) = 0.25

of the 125 Higgs signal strengths [50,51], as well as the projected *FCC-ee* sensitivity to $\delta\sigma_{Zh}$. For the latter two, Fig. 14 neglects the effect of radiative corrections in (5.14), which provides a conservative bound.

A more detailed analysis of the various sensitivities, including the effect of radiative corrections and dropping the above BR($h_2 \to h_1 h_1$) = 0.25 assumption (which is only justified in the limit $m_2 \gg v$), is shown in Figs. 15, 16 and 17 for $m_2 = 300$, 500, 700 GeV and $\sin\theta = 0.1,\ 0.05$, in the (a_2, b_3/v) plane. In these figures the theoretically allowed regions (recall Sect. 5.1) are shown as red points, while the points yielding a strongly first order EW phase transition (as discussed in Sect. 5.2) are depicted in green. We show the resonant di-Higgs production sensitivity of CLIC with $\sqrt{s} = 1.4$ TeV (orange) and $\sqrt{s} = 3$ TeV (blue) for a respective b-tagging efficiency of 70% (solid) and 90% (dashed), with CLIC able to probe the region not contained within each pair of sensitivity lines. For the case $\sin\theta = 0.1$ (for $\sin\theta = 0.05$ there is no sensitivity) we also show the HL-LHC sensitivity to the process $pp \to h_2 \to ZZ$ (see Sect. 3) as a shadowed yellow region. Figures 15, 16 and 17 also show the CLIC and *FCC-ee* reach of indirect probes[12] in the (a_2, b_3/v) plane for fixed m_2 and $\sin\theta$:

(i) The region where CLIC can access a deviation in the Higgs-self coupling w.r.t. the SM value, corresponding to $\delta\lambda_{111} = \left|(\lambda_{111} + \Delta\lambda_{111}^{1-\text{loop}}) - \lambda_{111}^{\text{SM}}\right| / \lambda_{111}^{\text{SM}} \geq 0.19$ (the tree-level and 1-loop contributions given respectively by (5.10) and (5.13)) is shown in Figs. 15, 16 and 17 as a dashed-black curve. We emphasize that a sizable Higgs self-coupling deviation $\delta\lambda_{111}$ generically features a strong correlation with a first order EW phase transition in theories beyond the SM (see e.g. [52,53]).[13]

(ii) The region where $\delta\sigma_{Zh}$ would be measurable with CLIC (*FCC-ee*) is shown in dark grey (light grey) in Figs. 15, 16 and 17. For $\sin\theta = 0.1$, such a measurement of $\delta\sigma_{Zh}$ at *FCC-ee* (or a similarly sensitive measurement of $\delta\sigma_h$ in VBF with CLIC) would yield the most pow-

[12] We note that the projected HL-LHC sensitivity to the singlet-doublet mixing $\sin\theta$ from a global fit to the measured 125 GeV Higgs signal strengths, given by $\sin\theta \simeq 0.18$ if negligible theory uncertainties are assumed [50], doe not allow to probe any parameter space region from Figs. 15, 16 and 17.

[13] However, there are exceptions to this, see [54].

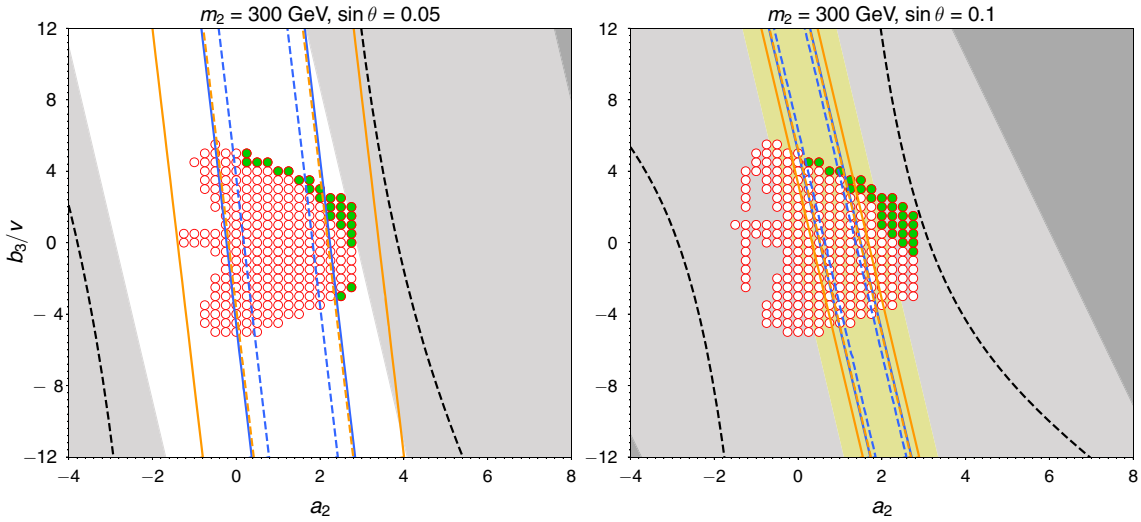

Fig. 15 Region of parameter space in $(a_2, b_3/v)$ for $m_2 = 300$ GeV and $\sin\theta = 0.05$ (left), $\sin\theta = 0.1$ (right) within the 95% C.L. sensitivity reach of resonant di-Higgs production searches at CLIC with $\sqrt{s} = 1.4$ TeV (orange) and $\sqrt{s} = 3$ TeV (blue) for a b-tagging efficiency of 70% (solid) and 90% (dashed): CLIC sensitivity region is that not contained within each pair of (sensitivity) lines. Overlaid are the SM + S points compatible with unitary, perturbativity and absolute stability of the EW vacuum from Fig. 10, and those yielding a strongly first order EW phase transition (green points). The dashed black lines correspond to the CLIC sensitivity to Higgs self-coupling deviations w.r.t. the SM $\delta\lambda_{111} = 0.19$. The yellow region (only for $\sin\theta = 0.1$) corresponds to the projected sensitivity of $pp \to h_2 \to ZZ$ searches at HL-LHC. The region within reach of a measurement of $\delta\sigma_{Zh}$ at CLIC (*FCC-ee*) is shown in dark (light) grey

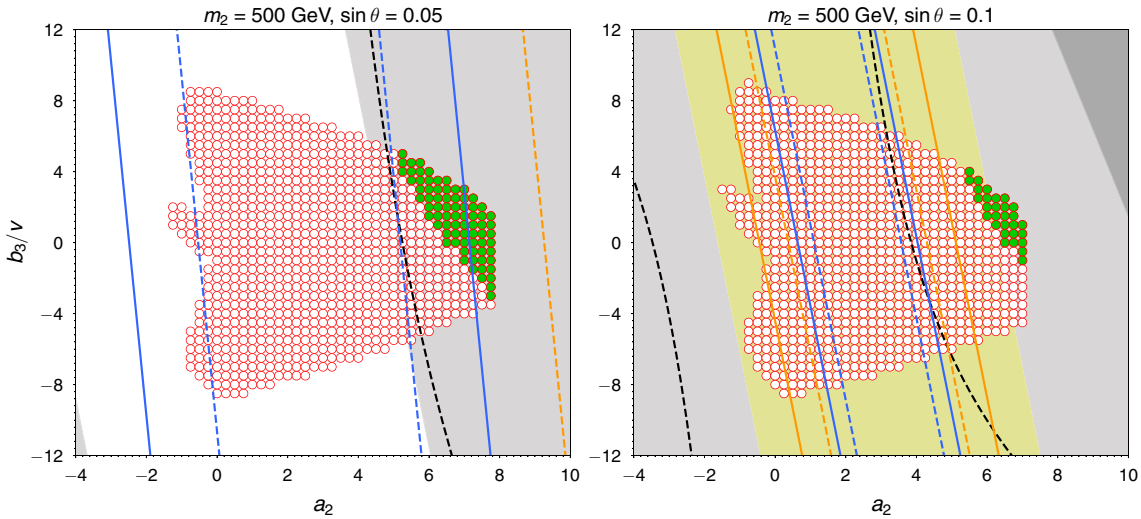

Fig. 16 Same as Fig. 15, but for $m_2 = 500$ GeV

erful constraint on the SM + S scenario, allowing to access the entire parameter space of the model. In contrast, for $\sin\theta = 0.05$ this measurement would yield a comparable sensitivity to that of the CLIC measurement of the Higgs self-coupling, and would be less sensitive than resonant di-Higgs searches at CLIC for masses $m_2 \lesssim 500$ GeV.

The results from Figs. 15, 16 and 17 also highlight that it would be possible in many cases to simultaneously access via direct and indirect collider probes the region of parameter space yielding a strongly first order EW phase transition in the SM + S scenario. This would allow to correlate the information from the various probes towards providing a robust test of the nature of the EW phase transition.

Before concluding, we emphasize that for a vanishing singlet-doublet mixing $\sin\theta \to 0$ (as is e.g. the case in the $\mathbb{Z}_2$ symmetric limit of the SM + S scenario) the resonant di-Higgs signature also vanishes, while the indirect probes $\delta\lambda_{111}$ and $\delta\sigma_{Zh}$ have their sensitivity significantly reduced (as deviations w.r.t. the SM only occur at 1-loop via the parameter a_2), particularly for low masses m_2. Yet in this

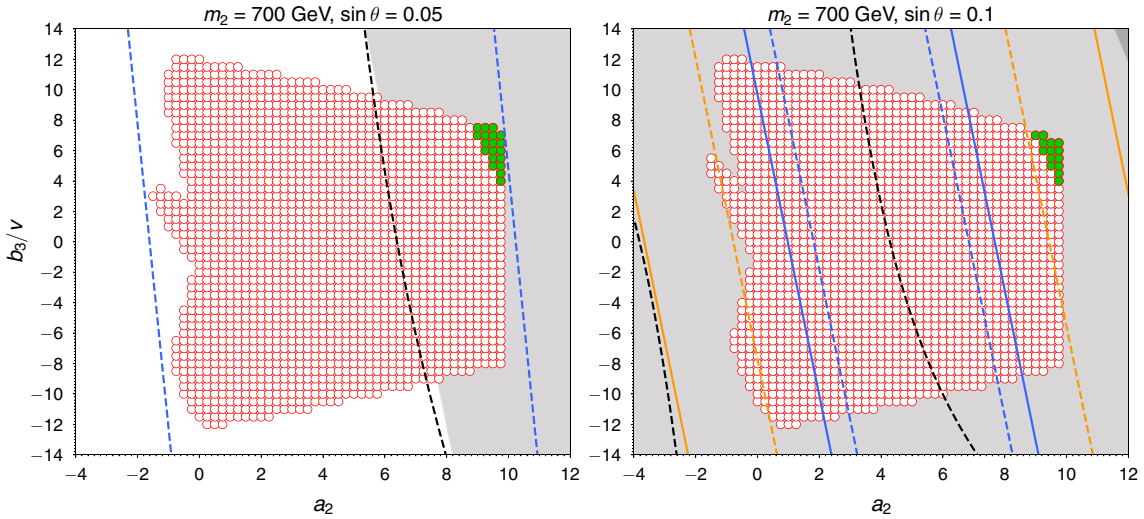

Fig. 17 Same as Fig. 15, but for $m_2 = 700$ GeV

limit a strongly first order EW phase transition is still possible [34,36,38]. The dominant probe of this parameter space region of the SM + S (the so-called "nightmare-scenario" for EW baryogenesis [38]) could be given by pair production of the singlet-like state h_2 [36] (except for the case of exact $\mathbb{Z}_2$ symmetry, h_2 would decay into SM states), and we note that a high-energy e^+e^- collider like CLIC could provide a tailored environment to analize the nature of the EW phase transition via such a process, a study we leave for the future (see also [55] for a preliminary study in this direction).

6 Conclusions

Among the primary goals of future collider facilities is the precise analysis of the properties of the Higgs sector. We have shown in this work that a high-energy e^+e^- machine like the proposed Compact Linear Collider – CLIC – operating at multi-TeV c.o.m. energies would yield very sensitive direct probes of the existence of new scalars, combining the energy reach with the clean environment of an electron-positron machine. In particular, resonant di-Higgs searches in the $4b$ final state at CLIC would surpass the reach of the HL-LHC by up to two orders of magnitude in the entire mass range $m_H \in [250\,\text{GeV},\ 1\,\text{TeV}]$. At the same time, these searches provide a direct avenue to probe the nature of the EW phase transition for non-minimal scalar sectors, and the possible origin of the cosmic matter-antimatter asymmetry via EW baryogenesis.

In the context of the extension of the SM by a real scalar singlet (SM + S, which could be viewed as a simple limit of the NMSSM or Twin Higgs theories), we have studied the sensitivity of CLIC to the parameter space where a strongly first order EW phase transition, as needed for successful baryogenesis, is realized. Our results show that there is a strong complementarity between direct searches for heavy Higgs bosons at CLIC via di-Higgs signatures, searches for heavy Higgses in di-boson (WW and ZZ) final states at both HL-LHC and CLIC, and indirect probes of BSM physics via measurements of the Higgs self-coupling λ_{111} and the Higgs associated production cross section σ_{Zh} at CLIC and other future colliders like *FCC-ee*. Combining the information from these searches could then allow to unravel the nature of EW symmetry breaking in the early Universe, and shed light on the origin of the baryon asymmetry of the Universe.

Acknowledgements We would like to thank Roberto Franceschini and Andrea Tesi for useful discussions and comments, and Ulrike Schnoor for guidance on the CLIC Delphes implementation. We also thank Dario Buttazzo, Diego Redigolo, Filippo Sala and Andrea Tesi for correspondence regarding their work [55]. J.M.N. is grateful to the Mainz Institute of Theoretical Physics (MITP) for its hospitality and its partial support during the completion of this work. J.M.N. was partially supported by the European Research Council under the European Unions Horizon 2020 program, ERC Grant Agreement 648680 (DARKHORIZONS) and by the Programa Atraccion de Talento de la Comunidad de Madrid under Grant 2017-T1/TIC-5202, and also acknowledges support from the Spanish MINECO's "Centro de Excelencia Severo Ochoa" Programme under grant SEV-2016-0597.

Data Availability Statement This manuscript has no associated data or the data will not be deposited. [Authors' comment: The manuscript has no associated data.]

Funded by SCOAP[3].

References

1. G. Aad et al. [ATLAS and CMS Collaborations], JHEP **1608**, 045 (2016). arXiv:1606.02266 [hep-ex]
2. The ATLAS collaboration [ATLAS Collaboration], ATLAS-CONF-2017-047 (2017)
3. CMS Collaboration [CMS Collaboration], CMS-PAS-HIG-17-031 (2017)
4. D.E. Morrissey, M.J. Ramsey-Musolf, New J. Phys. **14**, 125003 (2012). arXiv:1206.2942 [hep-ph]
5. M. Aicheler et al. https://doi.org/10.5170/CERN-2012-007
6. M.J. Boland et al. [CLIC and CLICdp Collaborations]. https://doi.org/10.5170/CERN-2016-004. arXiv:1608.07537 [physics.acc-ph]
7. S. Profumo, M.J. Ramsey-Musolf, G. Shaughnessy, JHEP **0708**, 010 (2007). arXiv:0705.2425 [hep-ph]
8. V. Barger, P. Langacker, M. McCaskey, M.J. Ramsey-Musolf, G. Shaughnessy, Phys. Rev. D **77**, 035005 (2008). arXiv:0706.4311 [hep-ph]
9. J.R. Espinosa, T. Konstandin, F. Riva, Nucl. Phys. B **854**, 592 (2012). arXiv:1107.5441 [hep-ph]
10. U. Ellwanger, C. Hugonie, A.M. Teixeira, Phys. Rep. **496**, 1 (2010). arXiv:0910.1785 [hep-ph]
11. Z. Chacko, H.S. Goh, R. Harnik, Phys. Rev. Lett. **96**, 231802 (2006). arXiv:hep-ph/0506256
12. G. Moortgat-Pick et al., Phys. Rep. **460**, 131 (2008). arXiv:hep-ph/0507011
13. J. Alwall et al., JHEP **1407**, 079 (2014). arXiv:1405.0301 [hep-ph]
14. T. Sjstrand et al., Comput. Phys. Commun. **191**, 159 (2015). arXiv:1410.3012 [hep-ph]
15. J. de Favereau et al., DELPHES 3 Collaboration. JHEP **1402**, 057 (2014). arXiv:1307.6346 [hep-ex]
16. https://github.com/uschnoor/delphes.git. Accessed 1 May 2018
17. N. Alipour Tehrani et al. CLICdp-Note-2017-001 (2017)
18. C.T. Potter. (2016) arXiv:1602.07748 [hep-ph]
19. M. Aaboud et al. [ATLAS Collaboration], Eur. Phys. J. C **78**, 293 (2018). arXiv:1712.06386 [hep-ex]
20. S. Heinemeyer et al. [LHC Higgs Cross Section Working Group]. https://doi.org/10.5170/CERN-2013-004. arXiv:1307.1347 [hep-ph]
21. M. Aaboud et al. [ATLAS Collaboration], Eur. Phys. J. C **78**(1), 24 (2018). arXiv:1710.01123 [hep-ex]
22. M.J. Dolan, C. Englert, M. Spannowsky, JHEP **1210**, 112 (2012). arXiv:1206.5001 [hep-ph]
23. D.E. Ferreira de Lima, A. Papaefstathiou, M. Spannowsky, JHEP **1408**, 030 (2014). arXiv:1404.7139 [hep-ph]
24. M. Cacciari, G.P. Salam, G. Soyez, Eur. Phys. J. C **72**, 1896 (2012). arXiv:1111.6097 [hep-ph]
25. M. Boronat, J. Fuster, I. Garcia, E. Ros, M. Vos, Phys. Lett. B **750**, 95 (2015). arXiv:1404.4294 [hep-ex]
26. CMS Collaboration [CMS Collaboration], CMS-PAS-HIG-17-009 (2017)
27. J.M. No, M. Ramsey-Musolf, Phys. Rev. D **89**(9), 095031 (2014). arXiv:1310.6035 [hep-ph]
28. S. Profumo, M.J. Ramsey-Musolf, C.L. Wainwright, P. Winslow, Phys. Rev. D **91**(3), 035018 (2015). arXiv:1407.5342 [hep-ph]
29. C.Y. Chen, S. Dawson, I.M. Lewis, Phys. Rev. D **91**(3), 035015 (2015). arXiv:1410.5488 [hep-ph]
30. T. Robens, T. Stefaniak, Eur. Phys. J. C **75**, 104 (2015). arXiv:1501.02234 [hep-ph]
31. D. Buttazzo, F. Sala, A. Tesi, JHEP **1511**, 158 (2015). arXiv:1505.05488 [hep-ph]
32. F. Bojarski, G. Chalons, D. Lopez-Val, T. Robens, JHEP **1602**, 147 (2016). arXiv:1511.08120 [hep-ph]
33. A.V. Kotwal, M.J. Ramsey-Musolf, J.M. No, P. Winslow, Phys. Rev. D **94**(3), 035022 (2016). arXiv:1605.06123 [hep-ph]
34. P. Huang, A.J. Long, L.T. Wang, Phys. Rev. D **94**(7), 075008 (2016). arXiv:1608.06619 [hep-ph]
35. T. Huang, J.M. No, L. Pernie, M. Ramsey-Musolf, A. Safonov, M. Spannowsky, P. Winslow, Phys. Rev. D **96**(3), 035007 (2017). arXiv:1701.04442 [hep-ph]
36. C.Y. Chen, J. Kozaczuk, I.M. Lewis, JHEP **1708**, 096 (2017). arXiv:1704.05844 [hep-ph]
37. I.M. Lewis, M. Sullivan, Phys. Rev. D **96**(3), 035037 (2017). arXiv:1701.08774 [hep-ph]
38. D. Curtin, P. Meade, C.T. Yu, JHEP **1411**, 127 (2014). arXiv:1409.0005 [hep-ph]
39. M. Chala, G. Nardini, I. Sobolev, Phys. Rev. D **94**(5), 055006 (2016). arXiv:1605.08663 [hep-ph]
40. H.H. Patel, M.J. Ramsey-Musolf, JHEP **1107**, 029 (2011). arXiv:1101.4665 [hep-ph]
41. L. Dolan, R. Jackiw, Phys. Rev. D **9**, 3320 (1974)
42. N.K. Nielsen, Nucl. Phys. B **101**, 173 (1975)
43. C.L. Wainwright, Comput. Phys. Commun. **183**, 2006 (2012). arXiv:1109.4189 [hep-ph]. https://github.com/clwainwright/CosmoTransitions. http://clwainwright.github.io/CosmoTransitions
44. H. Abramowicz et al., Eur. Phys. J. C **77**(7), 475 (2017). arXiv:1608.07538 [hep-ex]
45. T. Lastovicka, J. Strube, LCD-Note-2012-014 (2012)
46. J. de Blas et al., CERN Yellow Rep. Monogr. **3**, (2018). arXiv:1812.02093 [hep-ph]
47. M. Bicer et al. [TLEP Design Study Working Group], JHEP **1401**, 164 (2014). arXiv:1308.6176 [hep-ex]
48. D. d'Enterria, Frascati Phys. Ser. **61**, 17 (2016). arXiv:1601.06640 [hep-ex]
49. N. Craig, C. Englert, M. McCullough, Phys. Rev. Lett. **111**(12), 121803 (2013). arXiv:1305.5251 [hep-ph]
50. ATLAS-PHYS-PUB-2014-016 (2014)
51. The ATLAS collaboration [ATLAS Collaboration], ATLAS-CONF-2019-005 2019 (2019)
52. A. Noble, M. Perelstein, Phys. Rev. D **78**, 063518 (2008). arXiv:0711.3018 [hep-ph]
53. K. Hashino, M. Kakizaki, S. Kanemura, T. Matsui, Phys. Rev. D **94**(1), 015005 (2016). arXiv:1604.02069 [hep-ph]
54. A. Ashoorioon, T. Konstandin, JHEP **0907**, 086 (2009). arXiv:0904.0353 [hep-ph]
55. D. Buttazzo, D. Redigolo, F. Sala, A. Tesi, JHEP **1811**, 144 (2018). arXiv:1807.04743 [hep-ph]